High resolution emission spectroscopy of AlCl at 20 μ

H. G. Hedderich,[a] M. Dulick, and P. F. Bernath[b]
Centre for Molecular Beams and Laser Chemistry, Department of Chemistry, University of Waterloo, Waterloo, Ontario N2L 3G1, Canada

(Received 3 June 1993; accepted 17 August 1993)

The high resolution infrared emission spectrum of aluminum monochloride has been recorded with a Fourier transform spectrometer. A total of 1747 rovibrational transitions, $v=1\rightarrow0$ to $v=8\rightarrow7$, for the most abundant isotopomer $^{27}Al^{35}Cl$ and 708, $v=1\rightarrow0$ to $v=4\rightarrow3$, for the least abundant isotopomer $^{27}Al^{37}Cl$ have been assigned. This new set of infrared data was combined with existing microwave and millimeter-wave data to refine the Dunham Y_{ij} constants for the $X\,^1\Sigma^+$ electronic ground state. In addition two sets of mass-reduced Dunham U_{ij} constants have been determined from separate fits. In the first fit all of the U_{ij} constants that could be statistically determined were treated as adjustable parameters. In the second fit only the constants satisfying the condition $j<2$ were treated as adjustable parameters while the values for the remaining constants were fixed to constraints imposed by the Dunham model. Finally, in order to fully utilize the information provided by this extensive data set in an attempt to improve the prediction of energies for higher lying v, J levels of the $X\,^1\Sigma^+$ state, the combined data set, consisting of microwave, millimeter, and infrared (IR) data were fitted directly to the eigenvalues of the Schrödinger equation containing a parametrized internuclear potential energy function.

I. INTRODUCTION

There is chemical evidence suggesting that aluminum monohalides AlX (X=F, Cl, Br, I) are stable constituents present in aluminum–halogen systems at high temperatures.[1] They are easily produced in the gas phase by heating AlX_3 or a mixture of AlX_3 and Al.

The $A\,^1\Pi$–$X\,^1\Sigma^+$ transition of AlCl was observed in 1934 by Bhaduri and Fowler[2] in an electrical discharge of $AlCl_3$. Their tentative assignment of this transition was later confirmed by Holst[3] who performed a rotational analysis on a few bands of this transition. Further work was done in recording the electronic spectra both in emission[4–11] and in absorption,[12,13] followed by the recording of the microwave spectrum[14,15] and the millimeter-wave spectrum.[16] A compilation of the spectroscopic data can be found in Huber and Herzberg.[17]

Rogowski and Fontijn[18] measured the radiative lifetime of the $A\,^1\Pi$ state using laser-induced fluorescence while Rosenwaks was the first to observe AlCl chemiluminescence from the $Al+Cl_2$ chemical reaction.[19] In addition, results from *ab initio* calculations exist that yield information about the properties of the ground and excited electronic states.[20,21]

The spectra of AlCl are of astrophysical interest since AlCl has been detected in the envelope of the carbon star IRC+10216 by microwave spectroscopy.[22] In addition AlCl has also been detected via its $A\,^1\Pi$–$X\,^1\Sigma^+$ ultraviolet transition in the spectra of plumes from solid rockets;[23] AlCl is formed in the combustion of aluminum with an ammonium perchlorate oxidizer.

The dissociation energy of AlCl has been determined both from the predissociation[8] of the $A\,^1\Pi$ state and from thermochemical measurements.[24] A unique property of the $A\,^1\Pi$ state is the presence of a barrier to dissociation.[20,25]

In the infrared region only the matrix isolation spectrum[26,27] is known. Interestingly although AlCl is normally regarded as a high-temperature gas-phase molecule, it also exists as a stable amorphous solid below 180 K.[28] Vitreous solid AlCl disproportionates to $AlCl_3$ and Al metal when heated to a temperature above 180 K.

We report here the analysis of high resolution vibration-rotation emission spectra of $Al^{35}Cl$ and $Al^{37}Cl$ recorded with a Fourier transform spectrometer at 20 μ. The reduction of the data to spectroscopic constants is accomplished by fitting the data to the energy levels of a Dunham model and a parametrized potential energy model.

II. EXPERIMENT

High resolution infrared emission spectra of $Al^{35}Cl$ and $Al^{37}Cl$ were recorded with a Bruker IFS 120 HR Fourier transform spectrometer at the University of Waterloo at a resolution of 0.005 cm^{-1} with a liquid-helium-cooled Si:B detector and KBr beamsplitter. A cold filter attached to the Si:B detector limits the upper end of the spectral bandpass to 760 cm^{-1} while the combination of detector response and the transmission of the KBr beamsplitter effectively sets the lower limit to 350 cm^{-1}.

A mixture of $AlCl_3$ and Al powder was gradually heated in an alumina tube furnace to 1400 K at a rate of $\sim$5 K/min. The apparatus that was used in this experiment has already been described in detail in an earlier publication.[29] Deposition of solid material onto the KBr windows was prevented by adding argon buffer gas at a background pressure of 5 Torr. Lower resolution absorp-

[a]Present address: School of Earth and Ocean Sciences, University of Victoria, P.O. Box 1700, Victoria, British Columbia V8W 2Y2, Canada.
[b]Also at Department of Chemistry, University of Arizona, Tucson, Arizona 85721.

 0021-9606/93/99(11)/8363/8/$6.00

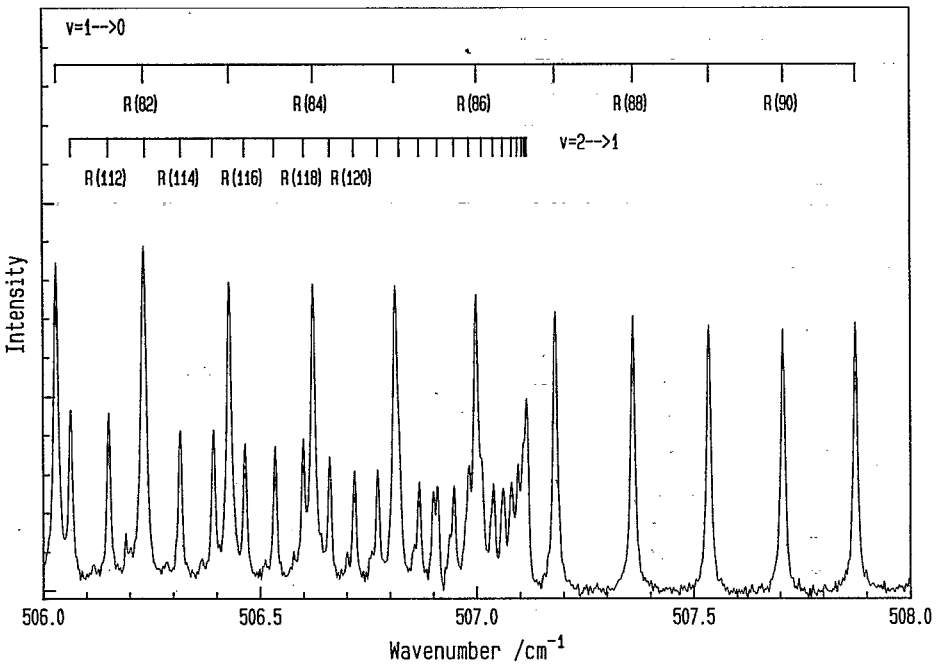

FIG. 1. Portion of the high resolution infrared emission spectrum of $Al^{35}Cl$ in the vicinity of the R-branch band head of the $v=2\rightarrow1$ band.

tion spectra were recorded up to a temperature of 1000 K in order to monitor for the appearance of AlCl. At temperatures above 1000 K the light source (globar) was switched off and emission spectra were taken. At 1000 K a weak emission feature around 480 cm^{-1}, attributed to AlCl, was observed. The intensity of the emission increased with increasing temperature until we finally recorded our spectra at 1400 K. Figure 1 shows a portion of the $Al^{35}Cl$ rovibrational emission spectrum observed at a temperature of 1400 K.

III. ANALYSIS

The spectral analysis program, PC-DECOMP, developed by Brault at the National Solar Observatory, was used in the data analysis where line centers are determined by fitting measured line profiles to Voigt line shape functions. For the strongest lines in the $Al^{35}Cl$ spectrum the signal to noise (S/N) ratio was typically 100 which allowed the positions of the lines to be determined to a precision of 0.0005 cm^{-1}. The line centers for the weaker lines, however, were determined only to ±0.001 cm^{-1} as a result of poorer S/N and in some instances blending with neighboring lines. The rotational lines were calibrated with respect to the pure rotational transitions of HCl which appeared as an impurity in the spectrum; the HCl lines were in turn calibrated relative to CO_2 lines in a previous experiment.[30] Assignment of rotational lines for $v=1\rightarrow0$ to $v=8\rightarrow7$ of $Al^{35}Cl$ and $v=1\rightarrow0$ to $v=4\rightarrow3$ of $Al^{37}Cl$ was facilitated by using an interactive color Loomis–Wood computer program.

The measured line positions are available from PAPS,[31] or from the authors upon request. Our data set was augmented by the addition of the $Al^{35}Cl$ and $Al^{37}Cl$ $J=1\leftarrow0$ pure rotational line frequencies that were measured using a pulsed molecular beam microwave spectrometer by Hensel *et al.*;[32] the frequencies of these lines, corrected for hyperfine structure, are also available from PAPS.[31] Included in these data[31] are the millimeter wave lines of Wyse and Gordy[16] that were used in our least-squares fits.

Data reduction of all the lines[31] to a set of spectroscopic constants was accomplished by using two different models, the Dunham model and the parametrized potential energy model, both of which are described below.

A. Dunham model

There are two conventional ways to fit the data to the parametrized (v,J) levels of a diatomic $^1\Sigma^+$ electronic state when more than one isotopomer exists. The first approach is to separately fit the rotational line frequencies of each isotopomer to the energy levels of the traditional Dunham model[33]

$$E_{vJ}=\sum_{i,j}Y_{ij}(v+\tfrac{1}{2})^i[J(J+1)]^j \qquad (1)$$

thereby obtaining a set of Dunham Y_{ij} constants for each isotopomer. The second approach entails the use of the alternate form

$$E(v,J)=\sum_{i,j}\mu^{-(i+2j)/2}U_{ij}(v+\tfrac{1}{2})^i[J(J+1)]^j \qquad (2)$$

with the reduced-mass dependence explicitly factored out in order to simultaneously reduce all isotopomer data to one set of mass-reduced Dunham U_{ij} constants.

The reduced-mass dependence of Eq. (2) is strictly valid only in the absence of Born–Oppenheimer break-

TABLE I. Dunham Y_{ij} constants for $Al^{35}Cl$ and $Al^{37}Cl$ in cm^{-1}.

	$Al^{35}Cl$	$Al^{37}Cl$
Y_{10}	481.774 655(196)	476.074 113(239)
Y_{20}	−2.101 811 2(876)	−2.052 564(107)
10^3Y_{30}	6.638 4(148)	6.421 2(139)
10^5Y_{40}	−2.025 5(830)	−1.931 326 69
10^1Y_{01}	2.439 300 66(12)	2.381 908 15(13)
10^3Y_{11}	−1.611 082 2(121)	−1.554 551 3(121)
10^6Y_{21}	4.691 92(358)	4.472 41(228)
10^9Y_{31}	−5.282(295)	−4.976 943 12
10^7Y_{02}	−2.501 711(190)	−2.384 823(250)
$10^{10}Y_{12}$	4.422 6(215)	4.182 5(323)
$10^{12}Y_{22}$	7.026(202)	8.096(429)
$10^{14}Y_{03}$	−4.652(338)	−6.055(366)
$10^{19}Y_{04}$	9.585(719)	8.713 942 34

down. An empirical first-order correction to Born–Oppenheimer breakdown[34] augments U_{ij} by a mass-dependent multiplicative factor

$$E(v,J)=\sum_{i,j}\mu^{-(i+2j)/2}U_{ij}[1+(m_e/M_A)\Delta_{ij}^{A}+(m_e/M_B)\Delta_{ij}^{B}](v+\tfrac{1}{2})^i[J(J+1)]^j. \quad (3)$$

In Eq. (3) the two atomic centers are labeled as A and B, m_e and M denote electron and atomic masses, respectively, and Δ_{ij}^{A} and Δ_{ij}^{B} are Born–Oppenheimer breakdown constants for atoms A and B. Watson[35,36] has since provided theoretical justification for the use of Eq. (3).

Values of Dunham Y_{ij} constants for $Al^{35}Cl$ and $Al^{37}Cl$ in Table I were obtained from separate isotopomer least-squares fits of all microwave, millimeter, and infrared (IR) lines.[31] Because the $Al^{35}Cl$ data set contains 1474 measured lines that involve levels over the ranges $0\leqslant v\leqslant 8$ and $0\leqslant J\leqslant 167$, a total of 13 Dunham Y_{ij} constants were statistically determined with all uncertainties in Table I quoted to one standard deviation. In contrast, because the natural abundance of $Al^{37}Cl$ is 24%, the data set for this isotopomer contains ~704 lines that involve vibrational levels only up to $v=4$, and as a result only 10 of the Dunham Y_{ij} constants were actually determined by the fit. The Dunham constants, Y_{31}, Y_{40}, and Y_{04}, were not determined in the $Al^{37}Cl$ fit but were determined in the $Al^{35}Cl$ fit. Rather than fixing the values of these parameters to zero, estimates of these parameters were obtained by using the relation

$$Y_{ij}=\mu^{-(i+2j)/2}U_{ij}$$

together with the U_{ij} values derived from a fit of all the data to Eq. (2).

Results from fitting the data to Eq. (3) are given in Table II under the column labeled "unconstrained fit." A total of 13 mass-reduced Dunham U_{ij} constants were determined where the i, j indices of the determined constants match those of their Y_{ij} counterparts from the $Al^{35}Cl$ fit. In addition, only two of the Born–Oppenheimer breakdown constants on the chlorine center, Δ_{10}^{Cl} and Δ_{01}^{Cl}, were determined. (Since only one naturally occurring isotope of aluminum exists, it is impossible to determine Δ_{ij}^{Al} directly by fitting the data.) Perhaps it should come as no surprise that Δ_{10}^{Cl} and Δ_{01}^{Cl} were the only Born–Oppenheimer constants determined; with a reduced mass of 15.2 one can expect minimal effects resulting from the breakdown of the Born–Oppenheimer approximation. The fact that our fit was even sensitive to Born–Oppenheimer breakdown is attributed mainly to the microwave and millimeter data.

TABLE II. Mass-reduced Dunham constants for AlCl in cm^{-1}. See text for an explanation of unconstrained and constrained fits.

	Unconstrained	Constrained
U_{10}	1 880.204 33(405)	1 880.202 16(282)
U_{20}	−32.012 71(111)	−32.012 10(103)
10^1U_{30}	3.954 99(770)	3.951 86(714)
10^3U_{40}	−4.861(173)	−4.802(161)
U_{01}	3.715 174 23(165)	3.715 174 08(165)
10^2U_{11}	−9.575 754 8(613)	−9.575 654 4(573)
10^3U_{21}	1.088 211(731)	1.087 167(714)
10^6U_{31}	−4.786(243)	−4.384(244)
10^5U_{02}	−5.802 349(362)	−5.802 142 65
10^7U_{12}	4.010 8(163)	3.872 177 11
10^8U_{22}	2.593 9(647)	2.840 097 61
10^9U_{32}		−1.377 413 77
$10^{10}U_{03}$	−1.964(101)	−1.576 868 16
$10^{11}U_{13}$		2.125 455 54
$10^{12}U_{23}$		−1.054 136 05
$10^{14}U_{04}$	6.208(339)	−0.357 487 25
$10^{16}U_{14}$		5.985 503 31
$10^{17}U_{24}$		−3.166 345 02
$10^{20}U_{05}$		3.852 400 49
$10^{20}U_{15}$		−1.355 155 50
$10^{24}U_{06}$		2.999 907 52
$10^{25}U_{16}$		−2.931 749 63
$10^{29}U_{07}$		5.148 207 33
$10^{34}U_{08}$		5.657 351 66
Δ_{10}^{Cl}	−1.293(137)	−1.223 8(951)
Δ_{01}^{Cl}	−1.442 7(287)	−1.443 2(287)

According to Dunham[33] all the coefficients in a power series potential are uniquely determined by the set of U_{i0} and U_{i1} constants. (In Dunham's original statement Y's were used rather than U's; this conclusion remains valid for the Y's if Born–Oppenheimer breakdown does not occur.) Consequently, only these two sets of constants are the "true" adjustable parameters in a fit. The remaining Dunham U_{ij} constants for $j\geqslant 2$ can all be expressed in terms of U_{i0}'s and U_{i1}'s. In other words, the functional dependencies of the U_{ij}'s for $j\geqslant 2$ in terms of U_{i0}'s and U_{i1}'s serve as constraints imposed by the Dunham model.

Up until now, only a few of the constrained U_{ij} relations exist in the literature,[36–38] some of which contain errors.[38] Recently, using symbolic computer algebra, Ogilvie[39] has managed to compile a complete set of constrained U_{ij} relations up to $0\leqslant i\leqslant 5$ and $2\leqslant j\leqslant 12$. These constrained U_{ij} relations now make it possible for the first time to carry out data reduction using a "true" Dunham model. The reason for emphasizing "true" is to draw attention to the fact that without these constraints in place, the U_{ij} constants determined from a fit lack physical meaning and serve merely as coefficients of a polynomial that reproduces the data. Dunham's intent was to formulate the (v,J) levels of a diatomic in such a way that the coefficients in the power series potential could be extracted directly from the

U_{ij}'s. A comparison of U_{ij}'s from unconstrained vs constrained fits provides more meaningful and reliable information about the properties of the internuclear potential as well as the effects due to perturbing electronic states.

Results from the fit that incorporated these constraints are shown in the second column of Table II (column labeled "constrained"). A simple comparison between the "unconstrained" and "constrained" U_{ij}'s seems to indicate for the most part very little difference between the two fits. In fact the standard deviation 0.793 for the constrained fit is just slightly higher than the standard deviation 0.790 for the unconstrained fit. However, the fact that the constrained fit involved 10 adjustable parameters as opposed to 15 for the unconstrained fit is a better indication of a superior fit with the constrained Dunham model which reproduces the data with a lesser number of degrees of freedom. With the exception of U_{04}, the agreement between these two sets of U_{ij}'s falls within 3 standard deviations; this leads us to conclude that the effects due to perturbing states are negligible. The disparity in the U_{04}'s in both sign and magnitude is more than likely due to a distortion in the unconstrained U_{04} that results from setting U_{14} and U_{24} to zero in the fit.

B. Parametrized potential model

Recording an IR emission spectrum under high resolution enables one to measure rovibrational line positions with extreme precision which translates to accurately mapping out the rovibrational energy level structure of the ground electronic state. Thus information derived from the data analysis will hopefully allow one to predict with reasonable accuracy rovibrational line positions involving higher lying (v,J) levels of the electronic ground state which lie outside the range of measurements. For instance, one reason for recording a "moderate temperature" IR spectrum of AlCl was to facilitate the assignment of AlCl lines observed in the "hot" spectra of rocket exhaust plumes and stellar atmospheres.

Unfortunately, the Dunham model is inadequate when it comes to extrapolating far beyond the range of experimental measurements. Although incorporation of constrained U_{ij} relations to the model improves the extrapolation capability of predicting the energies for high-J levels in a given vibrational state. The fact that the sole means of determining values for U_{i0}'s and U_{i1}'s involves fitting the data makes it virtually impossible to estimate the magnitude for higher U_{i0}'s and U_{i1}'s that cannot be determined from a fit of the data.

This inherent failure in the Dunham model has lead in recent decades to the development of a more sophisticated approach that entails fitting spectroscopic data directly to the eigenvalues of the Schrödinger equation containing a parametrized potential energy function. In this paper we shall refer to this method as the parametrized potential model. Kosman and Hinze[40] were the first to apply a variation of this method, "inverse perturbation analysis" (IPA), to spectroscopic data. Since then the efforts of several groups, notably Bunker and Moss[41] and more recently Coxon and Hajigeorgiou,[42,43] have lead to significant improvements in this method.

What makes the parametrized potential model so radically different from the traditional methods such as Dunham's model or Rydberg–Klein–Rees (RKR) inversion is that the adjustments in the parameters are now directly applied to the potential function rather than to a parametrized analytical expression approximating the eigenvalues of the potential. As a result, calculated eigenvalues are obtained by numerically solving the Schrödinger equation, and furthermore, the fit of the data to the model is now highly nonlinear in that we are now fitting the data in a sense to the solutions of a second-order differential equation.

A detailed description of the numerical methodology that is required in the development and implementation of this method will be reported in a forthcoming paper.[44] For now, only a brief outline of the method is given.

The effective radial Schrödinger equation for a diatomic $^1\Sigma^+$ electronic state[40] is

$$\left\{\frac{\hbar^2}{2\mu}\nabla^2 - U^{\text{eff}}(R) + E(v,J) - \frac{\hbar^2}{2\mu}[1+q(R)]J(J+1)/R^2\right\} \times \psi(R;v,J) = 0. \tag{4}$$

$U^{\text{eff}}(R)$ is an effective internuclear potential for vibrational motion where

$$U^{\text{eff}}(R) = U^{\text{BO}}(R) + U_A(R)/M_A + U_B(R)/M_B. \tag{5}$$

The first term on the right-hand side of Eq. (5), $U^{\text{BO}}(R)$, is the Born–Oppenheimer potential while the two remaining terms are corrections involving atomic centers A and B that effectively take into account Born–Oppenheimer breakdown (adiabatic effects) and homogeneous nonadiabatic effects from distant Σ electronic states. The inclusion of $q(R)$ in the rotational part of the radial Hamiltonian effectively treats J-dependent Born–Oppenheimer breakdown and heterogeneous nonadiabatic effects arising from distant Π states.

The Born–Oppenheimer potential $U^{\text{BO}}(R)$ is represented by the modified-Morse potential function

$$U^{\text{BO}}(R) = D_e\{1-\exp[-\beta(R)]\}^2/\{1-\exp[-\beta(\infty)]\}^2, \tag{6}$$

where

$$\beta(R) = z\sum_{i=0}^{n}\beta_i z^i, \tag{7}$$

$$\beta(\infty) = \sum_{i=0}^{n}\beta_i, \tag{8}$$

and

$$z = (R-R_e)/(R+R_e) \tag{9}$$

is one-half the Ogilvie–Tipping parameter.[45] For comparison the modified-Morse potential function used by Coxon and Hajigeorgiou[42,43] is

$$U^{\text{BO}}(R) = D_e\{1-\exp[-\beta(R)(R-R_e)]\}^2, \tag{10}$$

where

TABLE III. Internuclear potential energy parameters.

Parameter	Value	Uncertainty
	AlF	
D_e (cm^{-1})	56 000.0	
R_e (Å)	1.654 368 955 081 255	4.16×10^{-8}
β_0	4.561 393 094 342 520	3.93×10^{-7}
β_1	0.443 623 567 736 696	3.90×10^{-5}
β_2	0.799 452 956 164 073	2.58×10^{-4}
β_3	0.812 682 219 902 913	1.22×10^{-2}
β_4	11.799 285 785 710 51	9.88×10^{-2}
M_A (^{27}Al)	26.981 538 6	
M_B (^{19}F)	18.998 403 22	
	AlCl	
D_e (cm^{-1})	41 296.0	
R_e (Å)	2.130 143 506 503 515	5.21×10^{-8}
β_0	4.800 277 614 877 556	8.76×10^{-7}
β_1	1.085 629 063 448 244	3.46×10^{-5}
β_2	2.685 111 849 842 501	5.31×10^{-4}
β_3	13.445 749 711 038 98	1.01×10^{-2}
β_4	3.287 456 278 990 188	1.14×10^{-1}
u_1^B (cm^{-1} Å^{-1})	−87.721 710 312 334 99	1.61×10^{-1}
u_2^B (cm^{-1} Å^{-2})	73.927 232 877 379 11	1.73×10^{-1}
M_A (^{27}Al)	26.981 538 6	
M_B (^{35}Cl)	34.968 852 721	
M_B (^{37}Cl)	36.965 902 62	

$$\beta(R)=\sum_{i=0}^{n}\beta_i(R-R_e)^i. \tag{11}$$

Finally, following Coxon and Hajigeorgiou,[42,43] $U_A(R)$, $U_B(R)$, and $q(R)$ are represented by the power series expansions

$$U_A(R)=\sum_{i=1}^{n}u_i^A(R-R_e)^i, \tag{12}$$

$$U_B(R)=\sum_{i=1}^{n}u_i^B(R-R_e)^i, \tag{13}$$

and

$$q(R)=M_A^{-1}\sum_{i=0}^{n}q_i^A(R-R_e)^i+M_B^{-1}\sum_{i=0}^{n}q_i^B(R-R_e)^i. \tag{14}$$

Results from fitting the data to the parametrized potential model are displayed in Table III; only parameters that were statistically determined are listed along with their quoted 1σ uncertainties. An unphysically large number of digits are reported in Table III (and in Tables IV and V) as an aid for computer calculations. Our fits have highly correlated parameters so that additional digits beyond those indicated by the statistical uncertainty are necessary to reproduce our calculations. Rather than determining the number of digits necessary by trial and error, we simply report the complete computer output.

The standard deviation of the potential fit was 0.832. The thermochemical value for the dissociation energy D_e and the quoted atomic masses were obtained from Refs. 46 and 47, respectively. A plot of the isotopically invariant Born–Oppenheimer potential curve, Eq. (6), is displayed in Fig. 2.

TABLE V. Parameters from Coxon's form of $\beta(R)$ expansion for AlCl.

Parameter	Value	Uncertainty
D_e (cm^{-1})	41 296.0	
R_e (Å)	2.130 143 362 766 379	4.79×10^{-8}
β_0 (Å^{-1})	1.126 754 706 096 995	2.15×10^{-7}
β_1 (Å^{-2})	−0.204 688 770 518 025	2.17×10^{-6}
β_2 (Å^{-3})	0.068 413 468 119 424	5.92×10^{-6}
β_3 (Å^{-4})	0.012 807 450 385 511	3.83×10^{-5}
β_4 (Å^{-5})	−0.020 060 883 448 781	8.56×10^{-5}
u_1^{Cl} (cm^{-1} Å^{-1})	−87.657 211 608 196 41	1.49×10^{-1}
u_2^{Cl} (cm^{-1} Å^{-2})	74.347 402 261 888 67	2.21×10^{-1}

IV. DISCUSSION

As alluded to earlier, the aim of developing a parametrized potential model is to provide the means of extrapolating the energies of levels from an existing data set to predict with reasonably good accuracy the energies of higher lying (v,J) levels. Are the constants of Table III suitable for this purpose? Unfortunately, high-quality IR data for the high v's of the AlCl $^1\Sigma^+$ state does not currently exist and, therefore, a definitive answer must await the results from future experiments. Nevertheless, results from a fairly recent complete active space self-consistent field/multireference configuration interaction (CASSCF/

TABLE IV. Dunham potential parameters.

	Unconstrained Dunham model		Constrained Dunham model		Parametrized potential model	
Parameter	Value	Uncertainty	Value	Uncertainty	Value	Uncertainty
a_0					237 892.475 3	8.68×10^{-2}
a_1	−3.174 044 57	1.47×10^{-5}	−3.174 019 44	1.38×10^{-5}	−3.173 979 17	7.31×10^{-6}
a_2	6.848 702 60	2.03×10^{-4}	6.848 611 86	1.98×10^{-4}	6.849 605 64	7.25×10^{-5}
a_3	−11.707 189 00	2.05×10^{-3}	−11.709 401 94	1.91×10^{-3}	−11.741 977 16	4.59×10^{-4}
a_4	16.199 290 98	2.01×10^{-2}	16.217 471 00	2.01×10^{-2}	16.358 743 21	5.02×10^{-3}
a_5	−18.911 643 56	1.97×10^{-1}	−18.900 866 31	1.88×10^{-1}	−17.852 056 56	2.63×10^{-2}
a_6	26.795 745 94	8.48×10^{-1}	25.936 257 51	7.95×10^{-1}	12.289 855 21	8.77×10^{-2}
a_7					4.478 184 69	2.23×10^{-1}
a_8					−35.198 569 65	4.70×10^{-1}

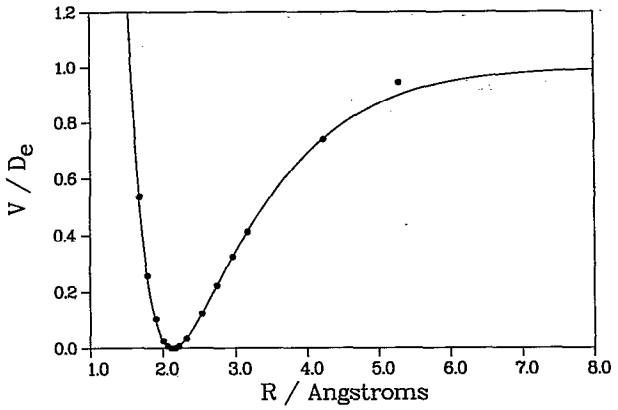

FIG. 2. Direct comparison of our AlCl Born–Oppenheimer potential (smooth curve) to the theoretical CASSCF/MRCI potential (discrete points) reported by Langhoff *et al.* (Ref. 20).

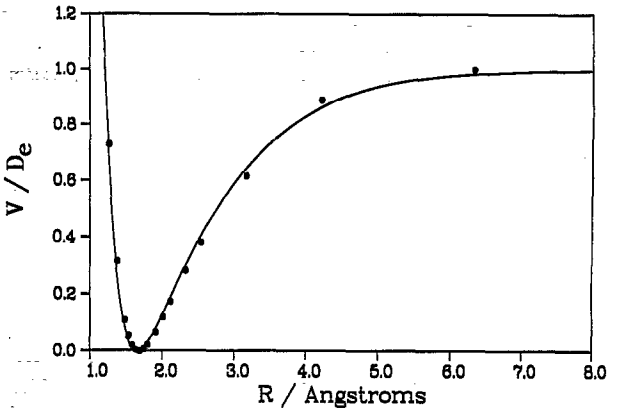

FIG. 3. Direct comparison of our effective AlF internuclear potential (smooth curve) to the theoretical CASSCF/MRCI potential (discrete points) reported by Langhoff *et al.* (Ref. 20).

MRCI) calculation by Langhoff *et al.*[20] together with a comparison involving the constrained Dunham model permit us to answer this question partially.

The points from the $^1\Sigma^+$ theoretical potential that are listed in Table II of Ref. 20 are reported as total energy. In order to add these points to the plot of our Born–Oppenheimer potential in Fig. 2 we subtracted the minimum total energy at $r\approx 4.10$ a.u. (2.17 Å) from each entry in the table followed by scaling these values to the total energy at $r=\infty$. (The authors in Ref. 20 did not report values of the potential past $r=10$ a.u.; however, using their calculated value of D_0, we managed to obtain an approximate estimate of the total energy at $r=\infty$.) The fact that these two potentials are in accord is one encouraging sign that the accuracy of the predictions by this model may extend well beyond the range of the measured data set.

Also included in Table III is a fit of our previously published AlF data[48] so that a similar comparison can be made between the potential derived by this model to the CASSCF/MRCI potential reported by Langhoff *et al.*[20] This comparison is illustrated in Fig. 3. The same procedure described above was used to scale the points of the theoretical potential in Table I of Ref. 20 to our potential with the exception that the entry at $r=50$ a.u. was arbitrally chosen to represent the total energy at infinite internuclear separation. Once again, we see that the agreement is exceptionally good. However, it should be noted that our AlF potential in the strict sense is not a true Born–Oppenheimer potential. Since only one natural isotope exists for both Al and F, the parameters that are associated with the Born–Oppenheimer breakdown could not be determined from the fit of spectral data involving the lone isotopomer $^{27}Al^{19}F$. But then again, with a reduced mass of 11.1 (as compared to 15.2 for AlCl), we can anticipate marginal effects arising from Born–Oppenheimer breakdown; therefore, in a realistic sense, the effective AlF potential derived from the fit is a reasonably good approximation to a Born–Oppenheimer potential. A similar argument can also be given for the effective AlCl potential as well.

Perhaps the most compelling evidence that demonstrates the predictive capability of the parametrized potential model is obtained from a comparison with the constrained Dunham model. With the aid of Eq. (15) from Ref. 33 the two sets of mass-reduced Dunham U_{ij} constants for $j=0$ and 1 in Table II were reduced to Dunham a_i potential parameters; a set of a's for each set of U_{ij}'s is listed in Table IV. The Born–Oppenheimer potential given by Eq. (6) is converted into a Dunham form through a power series expansion of $U^{\mathrm{BO}}(R)$ about $R=R_e$. Equating like $(R-R_e)^k$ terms from the Dunham and $U^{\mathrm{BO}}(R)$ expansions gives

$$a_0=\tfrac{1}{2}R_e^2[d^2U^{\mathrm{BO}}(R)/dR^2]_{R=R_e} \tag{15}$$

for $k=0$ and

$$a_k=a_0^{-1}R_e^{k+2}[d^{k+2}U^{\mathrm{BO}}(R)/dR^{k+2}]_{R=R_e}/(k+2)! \tag{16}$$

for $k>0$. The first few relations between the a's and β's are

$$a_0=\frac{D_e\beta_0^2}{2\{1-\exp[-\beta(\infty)]\}^2}, \tag{17}$$

$$a_1=-\frac{\beta_0^2+2\beta_0-2\beta_1}{2\beta_0}, \tag{18}$$

$$a_2=\frac{7\beta_0^4+36\beta_0^3+36(1-\beta_1)\beta_0^2+24(\beta_2-3\beta_1)\beta_0+12\beta_1^2}{48\beta_0^2}. \tag{19}$$

Values of the a_k's determined from Eqs. (15) and (16) are listed for $k\leqslant 8$ in Table IV. Quoted uncertainties for all three sets of a's were obtained by taking the square-root of the diagonal matrix elements of

$$\mathbf{J}^T\mathbf{C}\mathbf{J}, \tag{20}$$

where $\mathbf{C}$ is the covariance matrix obtained from either a Dunham or parametrized potential fit, $\mathbf{J}$ is the Jacobian matrix with elements

$$J_{kl}=\frac{\partial a_k}{\partial P_l}, \tag{21}$$

where P_l denotes either U_{ij}, β_i, or r_e, and $\mathbf{J}^T$ is the transpose of $\mathbf{J}$.

What makes the comparison in Table IV striking is that although the same data set were fitted to all three models, only the parametrized potential model is capable of estimating the a_i's at least to $i=8$ with statistical uncertainties that are in some instances an order of magnitude better than those determined from the constrained Dunham model. Table IV also indicates that the a's determined from the constrained Dunham model are only marginally better than those determined from the unconstrained model. Another way of viewing these results is to appreciate the fact that with all the a_i's determined up to $i=8$, this allows one to obtain good estimates of the adjustable U's up to U_{50} and perhaps as the trend in the uncertainties indicates, as high as U_{60}. In order to determine U_{60} from a conventional Dunham fit requires accessing levels that span $\sim 50\%$ of the potential well depth whereas the levels accessed by our measured data set span only a mere 13% of the well depth.

It is worth reemphasizing a point made earlier, that is, the parametrized potential model applies the adjustments directly to the parameters of the potential function. From a quantum mechanical perspective, by selecting a functional form for the Born–Oppenheimer potential that is qualitatively consistent with theory constrains the model to be physically reasonable beyond the range of the experimental data. Furthermore, using physical constraints to control the adjustment process, i.e., the Schrödinger equation in this case, rather than mathematically contrived constraints such as the constrained U_{ij} relations of the Dunham model, the results derived from this type of model reflect a highly refined physical representation of the molecular energy level structure.

There is no doubt that the variable-β Morse potential function introduced by Coxon to represent the isotopically invariant Born–Oppenheimer potential has led to a significant improvement in the parametrized potential model. However, there appears to be one particular aspect that may have been overlooked by Coxon, that is, the form of the $\beta(R)$ expansion must be carefully chosen in order to prevent the potential function from exhibiting nonphysical behavior at long range. The consequence of failing to prevent the potential function for exhibiting nonphysical behavior would negate the advantages afforded by the parametrized potential model; in particular, this would jeopardize the predictive capability of the model by imparting nonphysical effects to the solutions involving the higher lying vibrational-rotational levels.

The data set of AlCl is a prime example where $U^{\mathrm{BO}}(R)$ exhibits nonphysical behavior at long range when the Coxon–Hajigeorgiou form of the $\beta(R)$ expansion, given by Eq. (11), is used. A fit of the data using Eqs. (10) and (11) yielded the results given in Table V.

A plot of the Coxon–Hajigeorgiou form of $U^{\mathrm{BO}}(R)$ using the constants in Table V is displayed in Fig. 4; this figure clearly demonstrates that this form of $U^{\mathrm{BO}}(R)$ is unacceptable for $R \geqslant 4.0$ Å. The failure of $U^{\mathrm{BO}}(R)$ to exhibit the proper asymptotic form as $R \to \infty$ is traced to the $\beta(R)$ expansion [Eq. (11)] in which the last statistically determined parameter, β_4, is negative. As a consequence, $\beta(R)$ is a monotonically decreasing function of R that changes sign at $R=5.03$ Å. Had β_4 been positive, this would have made $\beta(R)$ a monotonically increasing function of R with $U^{\mathrm{BO}}(R)$ then having the qualitatively correct asymptotic form for large R.

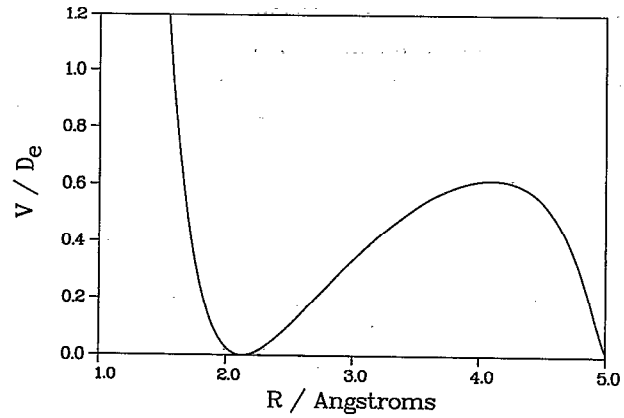

FIG. 4. The Coxon form of the Born–Oppenheimer potential for AlCl. This potential curve was generated using Eqs. (10) and (11) along with the parameter values listed in Table V.

Although the form of $U^{\mathrm{BO}}(R)$ given by Eq. (6) may appear as being somewhat awkward, it nevertheless has two built-in safeguards which prevent the possibility of nonphysical behavior from occurring at long range. By using an Ogilvie–Tipping variable as an alternative to the expansion variable $R-R_e$, $\beta(R)$ remains finite as $R \to \infty$. Therefore, the risk of premature numerical "blowup" of $\beta(R)$ is avoided. Second, if for some unforeseen circumstance $\beta(R)$ should become negative past some large value of R, the fact that we added the factor $\{1-\exp[-\beta(\infty)]\}^{-2}$ ensures that

$$\lim_{R\to\infty} U^{\mathrm{BO}}(R)=D_e$$

is strictly maintained.

V. CONCLUSION

Detection of infrared emission with a Fourier transform spectrometer is a very useful technique for recording high resolution rotation-vibration spectra of high temperature molecules. Advantages of this technique are wide spectral coverage (>1000 cm^{-1}), superb signal to noise spectra (S/N$\sim$100), and high precision measurements of spectral line positions (0.001–0.0001 cm^{-1}).

Data reduction of our IR data together with existing microwave and millimeter wave data to spectroscopic constants was accomplished in two ways. The first approach entailed fitting the spectral data to the energy levels of the Dunham model. The "conventional" Dunham fits yielded Y_{ij}'s for each isotopomer ($Al^{35}Cl$ and $Al^{37}Cl$) as well as a

set of isotopically invariant Dunham U_{ij} constants. A second set of U_{ij}'s was obtained from a fit where only the U_{i0}'s and U_{i1}'s were treated as adjustable parameters while the remaining U's were fixed to constraints imposed by the Dunham model.

The second approach employed a radically different model, the parametrized potential model, where data reduction is implemented by fitting spectral line frequencies directly to the eigenvalues of an effective radial Schrödinger equation containing a parametrized internuclear potential energy function. The motivation behind the second approach was to strive for accurate prediction of energies for higher lying rovibrational levels of the ground electronic state.

ACKNOWLEDGMENTS

This work was supported by the Phillips Laboratory/Propulsion Directorate, Edwards Air Force Base, CA, and the Natural Sciences and Engineering Research Council of Canada (NSERC). Acknowledgement is made to the Petroleum Research Fund, administered by the American Chemical Society, for partial support of this work. H.G.H. thanks the Deutsche Forschungsgemeinschaft for a postdoctoral scholarship. We also thank M. Gerry for providing microwave data prior to publication and J. Ogilvie for kindly providing us with his complete list of constrained Dunham U_{ij} relations.

[1] For example, P. Gross, C. Hayman, and D. L. Levy, Trans. Faraday Soc. **50**, 477 (1954).
[2] B. N. Bhaduri and A. Fowler, Proc. R. Soc. London, Ser. A **145**, 321 (1934).
[3] W. Holst, Z. f. Phys. **93**, 55 (1935).
[4] P. C. Mahanti, Z. f. Phys. **88**, 550 (1934).
[5] D. Sharma, Astrophys. J. **113**, 210 (1951).
[6] S. P. Reddy and P. T. Rao, Can. J. Phys. **35**, 912 (1957).
[7] A. K. Chaudhary and K. N. Upadhya, Ind. J. Phys. **42**, 549 (1968).
[8] R. S. Ram, S. B. Rai, K. N. Upadhya, and D. K. Rai, Phys. Scr. **26**, 383 (1982).
[9] Y. Kumar, B. N. Khanna, and D. C. Varshney, Ind. J. Pure Appl. Phys. **23**, 128 (1985).
[10] E. Mahieu, I. Dubois, and H. Bredohl, J. Mol. Spectrosc. **134**, 317 (1989).
[11] E. Mahieu, I. Dubois, and H. Bredohl, J. Mol. Spectrosc. **138**, 264 (1989).
[12] E. Miescher, Helv. Phys. Acta **8**, 279 (1934).
[13] E. Miescher, Helv. Phys. Acta **9**, 693 (1936).
[14] D. R. Lide, J. Chem. Phys. **42**, 1013 (1965); **46**, 1224 (E) (1967).
[15] J. Hoeft, T. Törring, and E. Tiemann, Z. Naturforsch. Teil A **28**, 1066 (1973).
[16] F. C. Wyse and W. Gordy, J. Chem. Phys. **56**, 2130 (1972).
[17] G. Herzberg and K. P. Huber, *Constants of Diatomic Molecules* (Van Nostrand–Reinhold, New York, 1979).
[18] D. F. Rogowski and A. Fontijn, Chem. Phys. Lett. **137**, 219 (1987).
[19] S. Rosenwaks, J. Chem. Phys. **65**, 3668 (1976).
[20] S. R. Langhoff, C. W. Bauschlicher, Jr., and P. R. Taylor, J. Chem. Phys. **88**, 5715 (1988).
[21] M. Wilson, M. B. Coolidge, and G. J. Mains, J. Phys. Chem. **96**, 4851 (1992).
[22] J. Cernicharo and M. Guélin, Astron. Astrophys. **183**, L10 (1987).
[23] W. K. McGregor, J. A. Drakes, K. S. Beale, and F. G. Sherrell, in Proceedings of the 27th Thermophysics Conference, July 1992, Nashville TN, paper AIAA-92-2917, AIAA (unpublished); J. A. Drakes (personal communication).
[24] D. L. Hildenbrand and L. P. Theard, J. Chem. Phys. **50**, 5350 (1959).
[25] R. F. Barrow, Trans. Faraday Soc. **56**, 952 (1960).
[26] H. Schnöckel, Z. Naturforsch. Teil B **31**, 1291 (1976).
[27] G. A. Olah, O. Farooq, S. M. F. Farnia, M. R. Bruce, F. L. Clouet, P. R. Morton, G. S. K. Prakash, R. C. Stevens, R. Ban, K. Lammertsma, S. Suzer, and L. Andrews, J. Am. Chem. Soc. **110**, 3231 (1988).
[28] M. Tacke and H. Schnöckel, Inorg. Chem. **28**, 2895 (1989).
[29] C. I. Frum, R. Engleman, Jr., and P. F. Bernath, J. Chem. Phys. **93**, 5457 (1990).
[30] G. Guelachvili and K. N. Rao, *Handbook of Infrared Standards* (Academic, Orlando, FL, 1986).
[31] See AIP documents no. PAPS JCPSA-99-8363-18 for 18 pages of tables. Order by PAPS number and journal reference from American Institute of Physics, Physics Auxiliary Publication Service, 500 Sunnyside Boulevard, Woodbury, New York 11797-2999. The price is $1.50 for each microfiche (60 pages) or $5.00 for photocopies of up to 30 pages, and $0.15 for each additional page over 30 pages. Airmail additional. Make checks payable to the American Institute of Physics.
[32] K. D. Hensel, C. Styger, W. Jaeger, A. J. Merer, and M. C. L. Gerry, J. Chem. Phys. **99**, 3320 (1993).
[33] J. L. Dunham, Phys. Rev. **41**, 721 (1932).
[34] A. H. M. Ross, R. S. Eng, and H. Kildal, Opt. Commun. **12**, 433 (1974).
[35] J. K. G. Watson, J. Mol. Spectrosc. **45**, 99 (1973).
[36] J. K. G. Watson, J. Mol. Spectrosc. **80**, 411 (1980).
[37] V. G. Tyuterev and T. I. Velichko, Chem. Phys. Lett. **104**, 596 (1984).
[38] R. Farrenq, G. Guelachvili, A. J. Sauval, N. Grevesse, and C. B. Farmer, J. Mol. Spectrosc. **149**, 375 (1991).
[39] J. Ogilvie (private communication); Comput. Phys. Commun. **30**, 101 (1983).
[40] W. M. Kosman and J. Hinze, J. Mol. Spectrosc. **56**, 93 (1975).
[41] P. R. Bunker and R. E. Moss, Mol. Phys. **33**, 417 (1977).
[42] J. A. Coxon and P. G. Hajigeorgiou, Can. J. Phys. **70**, 40 (1992).
[43] J. A. Coxon and P. G. Hajigeorgiou, Chem. Phys. **167**, 327 (1992).
[44] M. Dulick and P. F. Bernath (in preparation).
[45] J. F. Ogilvie, Proc. R. Soc. London, Ser. A **378**, 287 (1981).
[46] K. P. Huber and G. Herzberg, *Constants of Diatomic Molecules* (Van Nostrand–Reinhold, New York, 1979).
[47] I. Mills, *Quantities, Units and Symbols in Physical Chemistry* (Blackwell, Oxford, UK, 1989).
[48] H. G. Hedderich and P. F. Bernath, J. Mol. Spectrosc. **153**, 73 (1992).